

Precursors of fluidisation in the creep response of a soft glass

Raffaella Cabriolu^{*a}, Jürgen Horbach^b, Pinaki Chaudhuri^c and Kirsten Martens^d

Using extensive numerical simulations, we study the fluidisation process of dense amorphous materials subjected to an external shear stress, using a three-dimensional colloidal glass model. In order to disentangle possible boundary effects from finite size effects in the process of fluidisation, we implement a novel geometry-constrained protocol with periodic boundary conditions. We show that this protocol is well controlled and that the long time fluidisation dynamics is, to a great extent, independent of the details of the protocol parameters. Our protocol therefore provides an ideal tool to investigate the bulk dynamics prior to yielding and to study finite size effects regarding the fluidisation process. Our study reveals the existence of precursors to fluidisation observed as a peak in the strain-rate fluctuations, that allows for a robust definition of a fluidisation time. Although the exponents in the power-law creep dynamics seem not to depend significantly on the system size, we reveal strong finite size effects for the onset of fluidisation.

1 Introduction

Yield stress materials^{1,2}, although ubiquitous in everyday life, remain a challenging topic both for a fundamental physical understanding as well as for applied engineering problems. These materials are characterised by the feature that they behave solid-like for a small externally applied force, but can yield above a given yield stress either towards failure or towards a steady flow, depending on the brittleness of the material^{3,4}. One way to probe the complex response of these materials is to apply stresses, close to this yielding threshold, and study the transient dynamics preceding the yielding. Although macroscopic features of the yielding have been studied extensively for a long time, it is only recently that molecular dynamics simulations and scattering experiments have opened the way for a more microscopic understanding of the underlying processes, that lead to failure and flow, in such circumstances. This motivates our investigation of the creep dynamics of disordered materials using a microscopic approach, in order to reveal the physics involved and to search for possible signs of precursors. In this context, predicting the moment at which a material is going to yield is of course a very important goal, especially with respect to technical applications.

Many of these materials respond to an externally applied external load in the form of slow creep dynamics that can be succeeded either by complete arrest, catastrophic failure or rapid fluidisation. This observation is not only true for crystalline and amor-

phous hard solids, e.g. metallic systems, but has been reported as well in soft materials, such as dense emulsions and gels. In this context the measured macroscopic quantities of interest are usually the time-dependent deformation rate $\dot{\gamma}(t)$ and the fluidisation or failure time τ_f ^{5,6}. It is only relatively recent that the particular processes inducing the macroscopic creep dynamics have been also addressed on a more microscopic level. Experimentally this is possible for example by revealing the time evolution of spatially resolved plastic activity using dynamic light scattering techniques⁷ or confocal microscopy⁸. Another extremely insightful microscopic approach is of course the investigation of the creep and fluidisation using particle based simulations, which has been used both for dense particle systems⁹ and for network-forming gels¹⁰.

The occurrence of a yield stress implies the existence of a rigid solid. This rigid phase, however, does not correspond to an equilibrium state in the thermodynamic limit where the free energy of any phase of a system cannot depend on the shape of its boundary^{11,12}. Thus, solids that sustain a finite stress are in a non-equilibrium state and, provided that one waits long enough, they would eventually evolve into a stress-free state under the application of even an infinitesimal stress^{13–17}. The time associated with the approach of the latter equilibrium state may in general exceed any observable scales and, in this sense, rigid or yield-stress materials are very long-lived metastable systems. The transformation from a rigid solid to a stress-free solid in the limit of zero strain rate, $\dot{\gamma} \rightarrow 0$, is not well understood and in most cases this limit has to be inferred from an extrapolation from finite strain rates. Only in the case of a two-dimensional crystal, a recent computer simulation study¹⁷ demonstrated that the transformation from a metastable rigid crystal into a stress-free solid at finite strain rate are kinetic processes, associated with an underlying first-order

* E-mail: raffaella.cabriolu@ntnu.no

^a Department of Chemistry, Norwegian University of Science and Technology (NTNU), Høgskoleringen 5, 7491 Trondheim, Norway.

^b The Institute of Mathematical Sciences, Taramani, Chennai 600113, India.

^c Institut für Theoretische Physik II, Heinrich-Heine-Universität Düsseldorf, 40225 Düsseldorf, Germany.

^d Univ. Grenoble Alpes, CNRS, LIPhy, 38000 Grenoble, France.

phase transition at $\dot{\gamma} = 0$ and zero deformation. An example for such a kinetic process in crystalline materials is known as Andrade creep¹⁸, reflected by a power law of the strain rate as a function of the applied stress with an exponent close to 2/3. Of course, it remains to be shown how Andrade creep is exactly linked to the phase-ordering kinetics, thus being an analogue to spinodal decomposition in usual first-order transformations, such as liquid-gas or liquid-solid transitions.

In amorphous solids, the appearance of rigidity is due to a probable shift of the Newtonian regime to inaccessible long time scales, and there is not a similar underlying first-order phase transition in the limit $\dot{\gamma} \rightarrow 0$ as for the crystalline case¹⁷. Meanwhile, experiments and simulations studying creep in amorphous systems have found a variety of power-law exponents for the decay of the deformation rate, ranging between 1/3 and 1.0 (the latter value corresponding to logarithmic creep), with a multitude of values in-between^{8-10,19-23} (see also the extensive reviews of Bonn et al.²⁴ and Nicolas et al.²⁵). Thus, in the context of amorphous systems, the creep response shows a multitude of non-universal dependencies, notably on the preparation protocol prior to the application of the step stress (quench or pre-shear), on temperature, age and also on the dominant microscopic processes at play during the creep regime. In some network forming gel systems, the initial creep regime has been shown to be completely reversible and one expects the power-law creep to be a result of visco-elastic effects in a fractal gel network^{26,27}. On the other hand, there have been studies on the basis of molecular dynamics simulations explaining that the power-law creep in a variety of glassy systems can be related to a percolation of mobile regions and thus plasticity²⁸.

In a broader context, understanding and characterizing the physical mechanisms leading to observed rheological response of the amorphous materials in the vicinity of the yield stress threshold is of fundamental interest, with predictions of a dynamical transition at the threshold value. Therefore, the investigation of possible critical behaviour near the yield stress along with associated possible finite size effects, has been subject of many studies²⁹⁻³² but remains still a debated topic. One should note that some experiments have reported size effects in the measured value of threshold. In this context, a stress-controlled protocol at finite temperature allows for exploration of the creep response both above and below the threshold, as well as an investigation of possible precursors before complete fluidisation. Further, the idea of the underlying critical transition also motivates scrutiny of how system size influences the observed behaviour. For the case of applied shear rate, there have been diverse studies, looking at finite size effects, both in transient response and steady-state behaviour, but not much has been checked for applied stress situations.

One of the quantities of interest in the case of transient response, is the time-scale for fluidisation (or failure), τ_f , starting from an amorphous material at rest, and the results also vary and basically fall in two classes. Works on athermal creep in dense amorphous materials usually find power law scalings of the fluidisation time^{20,23} whereas thermally activated processes lead rather to an inverse exponential dependence³³⁻³⁶.

In this work we concentrate on thermally induced non-

reversible creep in dense disordered materials. Using an unconventional protocol combining a geometry imposed shear stress with periodic boundary conditions, we are able to disentangle finite size effects from boundary effects in the creep and fluidisation dynamics.

The article is structured as follows: In a first section we describe in detail the particle model, its rheological features and the novel protocol. We check in the second section for the robustness of this protocol with respect to the involved control parameters. Using extensive simulations averaging over a large number of realisations for different system sizes we then study the compliance curves as a function of the imposed shear stress which reveals the onset of plasticity in the transient response. The main result of our work concerns the study of the bulk dynamics prior to fluidisation. We show that the onset of fluidisation is accompanied by a maximum in the strain rate fluctuations, which one can interpret as a precursor to yielding. This feature allows to define in an unambiguous manner a fluidisation criterion and we find that the corresponding fluidisation time occurs at a given yield strain, which shows strong finite size effects. The last section is reserved for a detailed discussion of our results and the presentation of some ideas for potentially interesting future works.

2 Model and Scheme

For our study, we consider a three dimensional glass-forming 50:50 colloidal binary mixture, introduced in an earlier work by Zausch et al.³⁷. In this model, the colloidal particles, of species *a* and *b*, interact via the pair-wise Yukawa potential:

$$U_{1,2}(r) = \varepsilon_{1,2} d_{1,2} \frac{\exp(-k_{1,2}(r - d_{1,2}))}{r} \quad 1, 2 \in \{a, b\} \quad (1)$$

where, ε is the energy unit, d the diameter of the colloidal particle, k the screening length and r the distance between the two interacting particles. As in Ref.³⁷, the parameters are chosen as: $\varepsilon \equiv \varepsilon_{a,a} = 1.0$, $\varepsilon_{b,b} = 2.0\varepsilon$ and $\varepsilon_{a,b} = 1.4\varepsilon$, $d \equiv d_{a,a} = 1.0$, $d_{b,b} = 1.2d$ and $d_{a,b} = 1.1d$ and $k_{a,a} = k_{b,b} = k_{a,b} = 6/d$. Furthermore, colloidal particles of both types have same mass: $m_a = m_b = 1.0$. The potential is truncated at the cut-off distance $r_c^{a,b}$, where $U_{a,b}(r_c^{a,b}) = 10^{-7}\varepsilon_{a,b}$, i.e. negligibly small. The investigations are done for the particle density of $\rho_0 = 0.675m_a/d_{a,a}^3$. The choice of such parameters ensures that at densities ρ_0 and in the range of considered temperatures, neither crystallization nor demixing occurs. Four different sample sizes, with $N = 1600, 8000, 17576$ and 32768 number of particles in a cubic box were investigated.

In all the simulations, the ambient temperature is maintained via the Dissipative Particle Dynamics (DPD) thermostat³⁸. The system dynamics is then evolving according to the DPD equation of motion

$$\dot{\mathbf{r}}_i = \frac{\mathbf{p}_i}{m_i}; \quad \dot{\mathbf{p}}_i = \sum_{j(\neq i)}^N [\mathbf{F}_{i,j} + \mathbf{F}_{i,j}^D + \mathbf{F}_{i,j}^R], \quad (2)$$

where \mathbf{r}_i and \mathbf{p}_i are respectively the position and momentum of the particle *i* with mass $m_i = 1$, $\mathbf{F}_{i,j} = -\nabla(U_{i,j})$ is the force derivable by our Yukawa interaction potential, $\mathbf{F}_{i,j}^D$ is a dissipative force and $\mathbf{F}_{i,j}^R$ a random force. The dissipative force, $\mathbf{F}_{i,j}^D$, is propor-

tional to the velocity difference, $\mathbf{v}_{i,j} = \mathbf{v}_i - \mathbf{v}_j$ of particles i and j and it slows down the relative motion through a viscous effect controlled by the friction coefficient ξ :

$$\mathbf{F}_{i,j}^D = -\xi w^2(r_{i,j})(\hat{\mathbf{r}}_{i,j} \cdot \mathbf{v}_{i,j})\hat{\mathbf{r}}_{i,j}. \quad (3)$$

In the above equation, $\hat{\mathbf{r}}_{i,j}$ and $r_{i,j}$ are the unitary vector and the distance $|\mathbf{r}_i - \mathbf{r}_j|$ or module of the vector $\mathbf{r}_{i,j} = \mathbf{r}_i - \mathbf{r}_j$, respectively. The weight function $w(r_{i,j}) = \sqrt{1 - r_{i,j}/r_c}$ for $r < r_c^{DPD} = 1.2$, or $w(r_{i,j}) = 0$ otherwise. The relative velocities included in the DPD equations of motion ensure the correct thermostating of the system because of its ability to cancel the drifting velocity introduced by the shearing process and moreover this choice ensures Galilean-invariance and locally conservation of momenta. Concerning the role of the friction coefficient in the transient dynamics, it has been shown in previous works that there exists a range of values that does not affect neither the transient nor the microscopic dynamics^{9,37}, which we confirm also for our data in the following section. The random force

$$\mathbf{F}_{i,j}^R = \sqrt{2k_B T \xi} w(r_{i,j}) \boldsymbol{\theta}_{ij} \hat{\mathbf{r}}_{i,j}. \quad (4)$$

is implemented in the usual way with $\boldsymbol{\theta}_{i,j} = \boldsymbol{\theta}_{j,i}$ random Gaussian variables and a choice of the amplitude $\sqrt{2k_B T \xi} w(r_{i,j})$ obeying the fluctuation-dissipation relation³⁹.

We use the following protocol for preparing the glassy states, before applying the external shear stress: Initially, the colloidal liquid is equilibrated at $T = 0.20$ within standard periodic boundary conditions. We sample m independent equilibrium states within this NVT ensemble. Subsequently, all these m liquid samples are instantaneously quenched to a glassy temperature of $T = 0.05$, which is well below the mode coupling critical temperature ($T_c = 0.14$) for this binary mixture. Subsequently the samples are aged for a time $t_w = 10^4 \tau$. These aged quiescent states are then subjected to the external shear stress, to probe the response as explained in the following paragraph. In this work all sample averages are performed over $m = 80$ samples for the smallest size studied $N = 1600$ and $m = 40$ samples for the larger sizes $N = 8000$, 17576, 32768.

For the numerical study of the bulk response of our samples to an applied step in shear stress, we employ a novel shear protocol inspired by the work of Vezirov et al.⁴⁰, whereby a constant macroscopic shear stress σ_0 is maintained via a feedback control scheme, in a system with periodic boundary conditions. The feedback is implemented via an evolution equation for the macroscopic shear rate $\dot{\gamma}$:

$$\frac{d\dot{\gamma}(t)}{dt} = B[\sigma_0 - \sigma_{xy}(t)], \quad (5)$$

where σ_{xy} is the macroscopic shear stress, which is being maintained at a value σ_0 . We apply the shear along the x -direction, within the xy -plane. The adjustable damping parameter B is proportional to the inverse of the timescale for the bulk shear stress to relax to the imposed value. We need to choose B appropriately, such that the corresponding time-scale is smaller than any other involved time-scale to capture well the correct long time dynamics of the creep and the fluidisation of the material; the variations

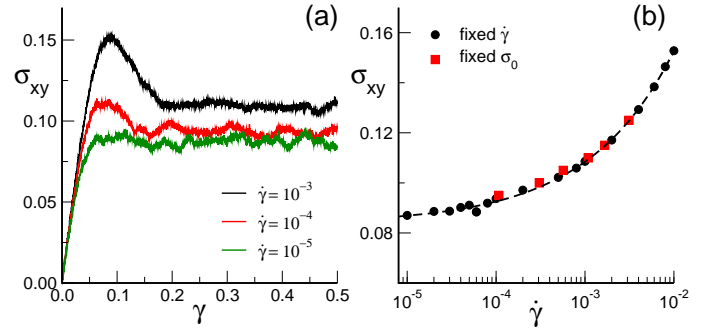


Fig. 1 (a) Shear stress σ_{xy} versus shear strain γ in a fixed shear rate protocol for the system with $N = 17576$ particles, shown for applied shear rates of $10^{-3}, 10^{-4}, 10^{-5}$. (b) Stationary value of the shear stress σ as a function of the applied shear rate $\dot{\gamma}$ in the fixed shear rate protocol (black circles), fitted with the Herschel-Bulkley function $\sigma_{xy} = \sigma_y + A\dot{\gamma}^n$, with $\sigma_y = 0.0836$, $A = 0.534$, $n = 0.444$ (dashed line). Superimposed is the data of the steady-state shear rate obtained from the imposed stress protocol imposing σ_0 (red squares).

in response with changing B will be discussed below. In the simulations we track positions and velocities of constituent particles and the shear stress is measured via the Irving-Kirkwood expression:

$$\sigma_{xy}(t) = \frac{1}{V} \left\langle \sum_i^N \left[m_i (v_{i,x}(t) v_{j,x}(t)) + \sum_{j>i}^N r_{ij,x}(t) F_{ij,y}(t) \right] \right\rangle. \quad (6)$$

The evolution of the system to applied stress is studied by simultaneously integrating, numerically, the equations of motion for the macroscopic shear rate given in Eqn. (5) and that of the individual particles given in Eqn. (2). The coupling of the two equations ensures that both the motion of the constituent particles as well as the macroscopic deformation simultaneously adjust to maintain the imposed stress σ_0 . Thus, along with the positions and velocities of the particles, the macroscopic shear rate, $\dot{\gamma}(t)$, and thereby the strain $\gamma(t)$, are dynamical relevant observables.

All the computations have been carried out using the open source molecular dynamics program from Sandia National Laboratories, LAMMPS,⁴¹ wherein we have implemented the scheme for integrating Eqn. (5). As in previous studies^{9,37}, we use a time step of $\delta t = 0.0083\tau$, where $\tau = \sqrt{md^2/\epsilon}$ is our unit of time.

3 Robustness of the novel protocol

To ascertain the range of stresses for which the rheology of the glass needs to be probed, we first reproduce the steady state flow response of the model at $\rho_0 = 0.675, T = 0.05$ obtained by imposing a usual shear protocol at imposed constant shear rate with periodic boundary conditions as shown in Fig. 1. It is well-known, that upon the application of a constant shear rate, the dense amorphous system initially responds macroscopically as an almost perfect elastic solid (with an elastic shear modulus G_0) before the macroscopic plasticity sets in. The load curve typically shows a stress overshoot, that will depend on the initial condition (age) of the quiescent material and the driving rate⁴²⁻⁴⁴, before entering a stationary state, where the macroscopic stress fluctuates around its steady state stress value σ . When plotted

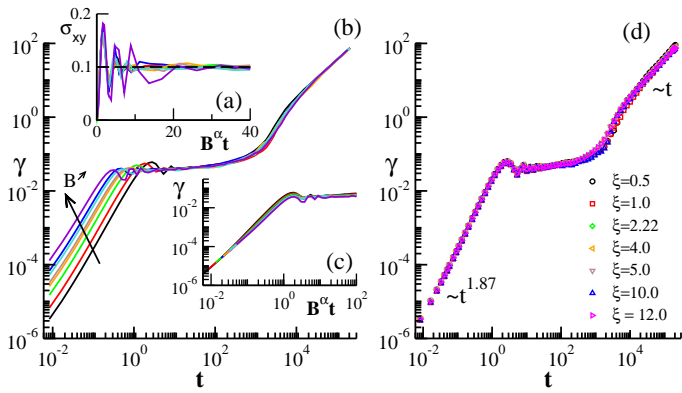


Fig. 2 For a system of $N = 17576$ particles, (a) evolution of bulk stress σ_{xy} for various damping parameters B (0.5, 1.0, 2.22, 4.0, 5.0, 8.0, 10.0, 20.0) in the shear rate evolution equation (Eqn. 5), under an applied step stress $\sigma_0 = 0.1$ at $t = 0$. (b) Corresponding strain evolution $\gamma(t)$ for the different values of B . (c) Zoom of the early time dynamics versus a rescaled time $B^\alpha t$, with $\alpha \approx 0.6$. (d) Effect of the friction coefficient ξ on the strain evolution $\gamma(t)$ for the system with $N = 17576$ colloidal particles under imposed stress $\sigma_0 = 0.1$ and damping factor $B = 0.5$.

against the applied shear rate $\dot{\gamma}$ the dependence of this steady state shear stress is well described by a phenomenological generalized Herschel-Bulkley type fit $\sigma = \sigma_y + A\dot{\gamma}^l$. Thus, the flow curve provides us the range of values, relative to the yielding threshold, that one can explore to study the response to the externally applied stress.

To test the robustness of our protocol against the various control parameters, we consider now one such stress value within that range, viz. $\sigma_0 = 0.1$, to study the dynamics using the feedback protocol that we have outlined earlier (Eqn.5). At first, we check how the choice of the damping parameter B in Eqn.5 influences the observed behaviour. For a quiescent glass, i.e. when there is no external shear, the time-averaged shear stress σ_{xy} is zero. At time $t = 0$, when the external shear stress is suddenly set to a finite value, the bulk shear stress σ_{xy} of the material starts to adjust to the externally imposed one. This evolution is illustrated in Fig. 2(a) for various values of the damping parameter B . As expected, the long time bulk shear stress equals the applied magnitude, indicating that the protocol is working fine. At early times, we observe that $\sigma_{xy}(t)$ initially increases, responding to the external forcing, and then oscillates as the feedback mechanism kicks in before settling down to σ_0 . The magnitude and lifetime of the observed oscillations is naturally determined by our control parameter B .

The corresponding evolution of the bulk shear strain of the system $\gamma(t)$ is shown in Fig. 2(b); each curve is averaged over 10 independent trajectories, starting from different initial glassy configurations, as explained in the model section. Firstly, the overall behaviour of $\gamma(t)$, as obtained via the feedback control, is similar to what is observed in experiments⁴⁵, thus validating the numerical scheme. We also observe that the damping factor B has an influence only at short-times ($t < 10$) till around the occurrence of the transient overshoot in $\gamma(t)$, with the magnitude of B determining the location and height of the overshoot. The larger the value

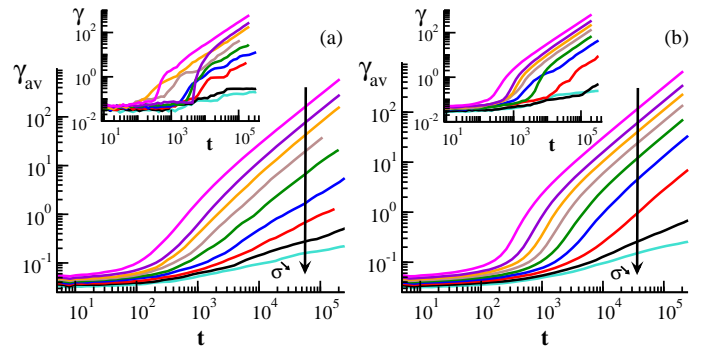


Fig. 3 Strain evolution $\gamma(t)$ for a range of imposed stresses σ_0 (0.080, 0.085, 0.090, ..., 0.125), each averaged over an number of different initial conditions for (a) the smallest system ($N = 1600$) and (b) the largest system ($N = 17576$) studied. The inset shows typical curves for corresponding individual runs.

of B , the earlier the system reaches the overshoot and the subsequent creep regime, which is consistent with the consideration that the damping factor is inverse to the resistance of the material at the given deformation. On the other hand, the choice of B does not have any effect on the response at later times ($t > 10$). We see that the regime where the deformation $\gamma(t)$ shows a plateau, indicative of the elastic response of the material⁴⁵, depends only on the stress imposed, that is in fact the same for each curve in Fig. 2(b). Similarly, the late time steady state regime, $\gamma(t) \sim t$, and its onset is also not altered by the magnitude of B . In Fig. 2(c), we show the time-scaled shear strain for the different B factors. We observe that the data collapse for the early time dynamics for a rescaling of time with a factor proportional to B^α with an empirical scaling exponent $\alpha \approx 0.6$. This rescaling also shows that the initial slope for $t < 1$ is the same for all the curves with dynamics that are close to ballistic motion with $\gamma(t) \sim t^{1.87}$. Note that the data for the early growth of stress in the system, can also be collapsed, using the same time rescaling, as shown in Fig.2(a). These short-time damped oscillations result from a competition of inertia of the stress regulation and the systems elastic properties, an effect that is also commonly observed in experiments where this ringing effect emerges from a coupling of the instrument inertia and the elasticity of the material^{46–48}.

To be complete, we also check whether the DPD friction coefficient ξ has any influence in the strain evolution. The response for various values of ξ at a given target stress σ_0 and damping factor B is shown in Fig. 2(d). We see that the dynamics appear insensitive in the range of values of ξ examined: both fluidization time and the creep regime are identical for the six different friction coefficients investigated. Further we also checked that the empirical scaling exponent of B does not depend on the specific value of the friction coefficient ξ (data not shown here). In all the subsequent data analysis of the following sections we fixed $B = 1$ for the damping factor and $\xi = 12^{37}$ for the friction coefficient, knowing that all the long time results will not crucially depend on these values.

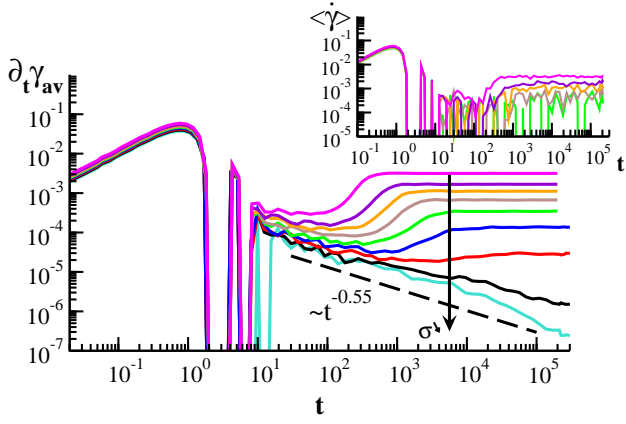


Fig. 4 The time derivative of the averaged strain response $\partial_t \gamma_{av}$ as a function of time, obtained from the data shown in Fig.3(b) for the same range of stresses. The inset shows the time evolution of the average shear rate that we obtain directly from our protocol (see Eqn. 5), $\langle \dot{\gamma}(t) \rangle$, averaged over the ensemble of 40 initial states, for $N = 17576$ and $\sigma_0 = 0.115, 0.110, 0.105, 0.100$. The data of smaller stresses is not shown here due to the strong fluctuations despite averaging.

4 Creep response

We now systematically discuss the response of the model system, for different magnitudes of the imposed target stress σ_0 . Fig. 3 shows the evolution of the strain response $\gamma_{av} = \langle \gamma(t) \rangle$ for a range of stresses for a system with (a) $N = 1600$ particles, averaged over the ensemble of $m = 80$ initial states, and (b) $N = 17576$ particles, averaged over the ensemble of $m = 40$ initial states. In the inset of either figure, we show some of the individual trajectories for the strain response $\gamma(t)$, obtained from one specific initial state within the ensemble for the different applied stresses. First focusing on the ensemble-averaged γ_{av} , we observe that for $\sigma_0 > 0.095$, we observe the long-time steady state regime $\gamma_{av}(t) \sim t$. For smaller applied stresses, at these long times ($t > 10^4$), the material creeps, i.e. $\gamma_{av}(t) \sim t^\beta$ ($\beta < 1$), till the longest accessible time-scales.

If one focuses on the macro-response of a single system, as shown in the insets, we can discern a difference in response. The strain curves for the smaller system ($N = 1600$) demonstrate sharper onset of flow, compared to the larger system ($N = 17576$), indicating already the existence of finite size effects in the fluidisation process. Further, signatures of stick-slip motion⁴² are also visible in the smaller system, i.e. there are time windows over which the deformation remains nearly constants, interspersed with intermittent jumps. This becomes more prominent as one goes to smaller σ_0 , i.e. in the approach to the yield stress threshold, especially where the long time linear regime in the flow response (i.e. $\gamma(t) \sim t$) is not yet visible. Such intermittency is less visible in the data, for the larger system, due to the spatial average of response over many smaller intrinsic blocks. Further, the stick-slip behaviour is averaged out, while calculating ensemble averages. Note that such intermittent behaviour is consistent with the idea of strongly correlated avalanche dynamics occurring close to the yielding threshold.

Additionally, in Fig. 4, we show the corresponding behaviour of the shear rate $\dot{\gamma}(t)$, computed in two different ways. In the inset

of Fig. 4, we show the time evolution of the ensemble-averaged $\langle \dot{\gamma} \rangle$ as directly measured from our numerical integration, for a range of applied stresses. For the larger values of σ_0 , a long-term steady state is visible, i.e. $\langle \dot{\gamma} \rangle$ fluctuates around a constant value. However, below a certain σ_0 , the data becomes too noisy, for the averaging done over the ensemble of $m = 40$ initial states. On the other hand, if one considers the numerical derivative of the ensemble-averaged strain $\langle \gamma(t) \rangle$ (from Fig.3(b)), as is usually done in experiments^{6,45}, we are able to discern the response $\partial_t \gamma_{av}$ at all the values of σ_0 with reasonable precision, as shown in the main figure of Fig. 4. For σ_0 below a certain value, $\partial_t \gamma_{av}$ is not constant at long times, i.e. there is no observed steady-state regime. Rather, we observe that $\partial_t \gamma_{av}$ decreases with time in a power law fashion, $\partial_t \gamma_{av} \sim t^{\beta-1}$; i.e. the material is creeping as expected.

To counter-check our results, we gather the data for the measured steady-state $\dot{\gamma}$ for the different applied σ_0 (for which a steady state can be reached) to compare with the shear-rate imposed data. As we can see in Fig.1(b), the data from the two different protocols, applied fixed shear rate and applied fixed stress, are statistically consistent, as it should be, thereby, confirming again the validity of the numerical scheme used to impose a fixed target shear stress.

5 Precursors of fluidisation: finite size effects

Another quantity that is particularly useful to study the onset of plasticity in the time-dependent mechanical response is the compliance $J(t) = \gamma(t)/\sigma_0$ ⁴⁹. In the left panel of Fig. 5, for various imposed stresses σ_0 , the data for $J(t)$ is shown for the system size of $N = 17576$ particles, from which, different features can be observed. For all the curves, there is a common region at early times ($t \sim [10^{-2} - 10^1]$), where all the data superimpose for the entire range of applied σ_0 that we have studied. This is the regime of elastic deformation and it depends only on the material itself (in our case, the interactions and/or the dissipation processes). At later times the curves start to separate out, at time-scales which increase with decreasing σ_0 , due to the dependence of the plastic response on the magnitude of imposed stress. The main plot nicely shows the superposition of all the compliance curves at short times, where the dynamics remains completely reversible, after which deviations start occurring, with a strong dependence on the imposed target stress σ_0 . To make the separation of the different curves better visible, we also plot the time derivative of the compliance as a function of the compliance itself as shown in the inset of the left panel of Fig. 5. The strong drop of the time derivative of the compliance at a value of the compliance of $J \approx 0.5$ marks the onset of plasticity, beyond which, all the curves start to depart from the regime of elastic response. Thus, in such a manner, we are able to delineate the elastic and plastic regimes of the response, after the application of the external shear stress.

Thereafter, we check how the size of the system affects the compliance. This is shown on the right panel of Fig. 5, for three different values of applied stress, viz. $\sigma_0 = 0.125, 0.100, 0.090$. For the largest applied stress, there is no difference in the response

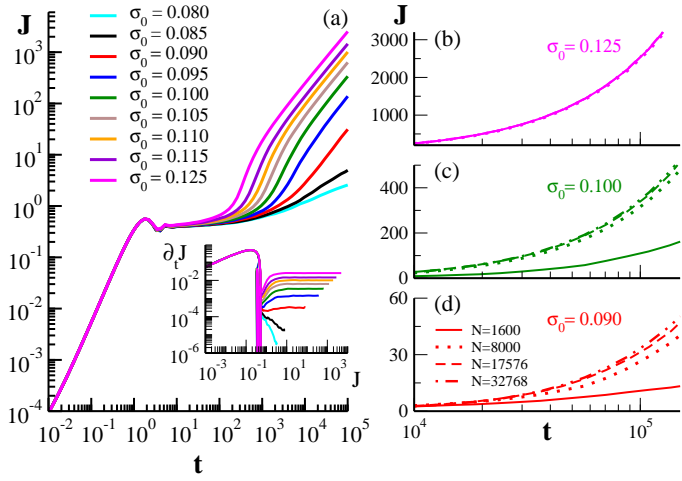


Fig. 5 (a) Evolution of compliance $J(t) = \gamma(t)/\sigma_0$ for the system with $N = 17576$ particles, for the range of imposed stresses explored. The inset shows the time derivative of the compliance $\partial_t J$ as a function of the compliance J . (b) The compliance $J(t)$ for $N = 1600, 8000, 17576, 32768$, for $\sigma_0 = 0.090, 0.100, 0.125$.

across system sizes. As we go to lower stresses ($\sigma_0 = 0.100$), the difference starts to be visible, with the compliance curve for the smallest system ($N = 1600$) displaying a slower increase. The difference across the other sizes becomes more prominent when one goes even lower in stress ($\sigma_0 = 0.09$). Thus, one can conclude that finite size effects are present in the macroscopic response and this effect becomes more significant as we approach the yield stress threshold.

To identify possible precursors of fluidisation, we consider now the sample-to-sample variations in the mechanical response within the ensemble of initial states⁹. This is quantified by measuring the time-dependent fluctuations in strain, $\Delta\gamma_i(t)$, of the configuration i in the ensemble, relative to the ensemble-averaged strain curve $\langle\gamma(t)\rangle$:

$$\Delta\gamma_i^2(t) = \frac{[\gamma_i(t) - \langle\gamma(t)\rangle]^2}{\langle\gamma(t)\rangle^2} \quad (7)$$

where $\gamma_i(t)$ is the strain evolution curve for the configuration i . Similar measurements have been employed in experiments, albeit considering fluctuations across different regions in the sample⁵⁰. In Fig. 6(a), we show how the corresponding ensemble-averaged fluctuations $\langle[\Delta\gamma^2(t)]\rangle$, behave with varying σ_0 , measured over $m = 40$ configurations for the system size $N = 17576$. As we can see, the function is typically non-monotonic⁹, with very little deviations among samples in the elastic regime and again negligible when all samples are fluidised. In between, there is a maximum whose locations shifts to longer timescales, with decreasing σ_0 , a trend very similar to what we discussed for fluidisation timescales in the above discussion related to measured compliances, $J(t)$, shown in Fig. 5.

The short time elastic response is reflected as well in the sample to sample fluctuation of the strain. In Fig. 6(b), we plot the rescaled fluctuations, i.e. multiplied by σ_0^2 , versus the compliance (J), and find again a perfect collapse of the data up to the compliance value $J = 0.5$, which is where plasticity sets in. In Fig. 6(c),

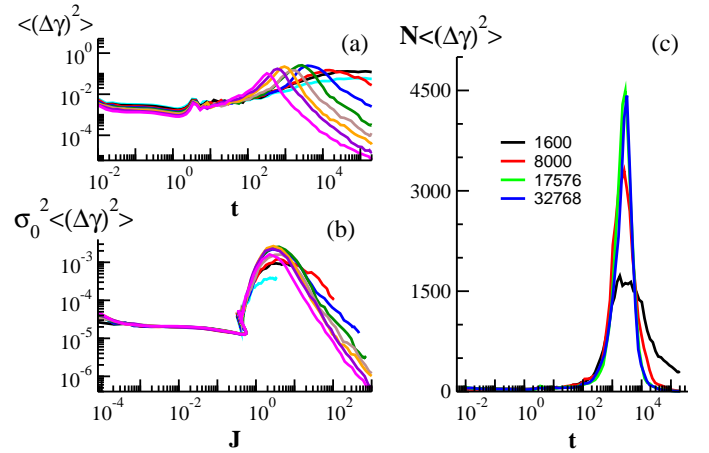


Fig. 6 (a) Time evolution of sample to sample fluctuations in strain $\langle[\Delta\gamma^2(t)]\rangle$, for different applied σ_0 , for $N = 17576$. (same as in Fig. 5) (b) Corresponding rescaled fluctuations $\langle[\Delta\gamma^2(t)]\rangle\sigma_0^2$ as a function of the compliance $J = \langle\gamma\rangle/\sigma_0$. (c) System size rescaled sample to sample fluctuations in strain $\langle[\Delta\gamma^2(t)]\rangle$ as a function of time for different system sizes N .

we plot for a given stress $\sigma_0 = 0.1$, the strain fluctuations, as a function of time, for different system sizes; to make better comparison, we plot $N\langle\Delta\gamma^2\rangle$. We find that the size dependence in the peak of the strain fluctuations is scaling in a non-trivial manner with system size. This, again, hints at system size effects in the fluidisation process, consistent with our earlier analysis related to the compliance curves.

To obtain a rigorous criterion for the fluidisation, we now concentrate on the late time fluidisation regime. For this, we study in detail the location of the peak in the fluctuations, which we interpret as a precursor to steady state fluidisation. In Fig. 7(a), we plot the sample to sample strain fluctuations, $N\langle\Delta\gamma^2\rangle$, now as a function of strain γ . We find that for all imposed stresses, for which the system eventually shows steady flow, the maximum of these fluctuations occurs at approximately the same strain, $\gamma_y \approx 0.3$, suggesting a yield strain criterion for the fluidisation process. We use this yield strain to define in an unambiguous manner the fluidisation time, τ_f , by monitoring at what time the strain response $\gamma(t)$ is reaching this value of γ_y for any applied σ_0 .

The results of this procedure are displayed in Fig. 7(b), where we plot, using open symbols, the fluidisation time τ_f as a function of applied stress σ_0 for different system sizes. In the literature one finds different propositions for the dependency of the fluidisation time on the applied external stress, that can take either an exponential form or a power law divergence²⁵. Note that the precision of our data is not sufficient to discriminate between these two propositions. Here, we decided to fit the data with a diverging function of the form $\sim [\sigma_0 - \sigma_s]^{-\zeta}$, and we find that the yielding threshold σ_s decreases with system size, viz. we find the following estimates for the yield stress: $\sigma_s \approx 0.0772(N = 17576), 0.0801(N = 1600)$, using $\zeta = 2.66$.

An alternative simple definition for onset of fluidization would be the time when the onset of steady state flow occurs, i.e. when $\gamma(t)$ becomes constant. Using data shown in Fig. 4 for $\partial_t \gamma_{av}$, we are able to identify this timescale (τ_f^{ss}) for $N = 17576$, and this too is

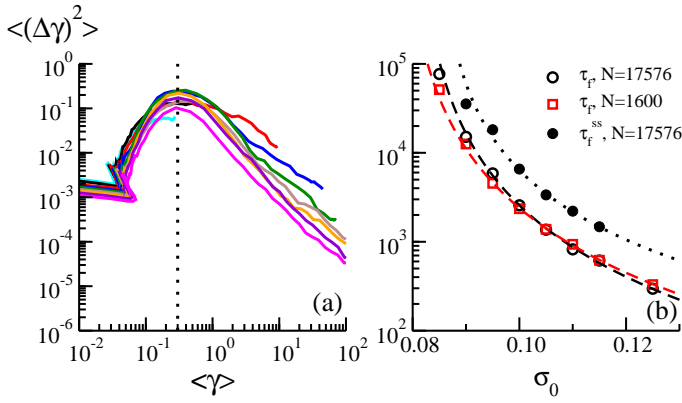


Fig. 7 (a) Sample to sample fluctuations in strain $\langle[\Delta\gamma^2(t)]\rangle$ as a function of strain γ . (b) Fluidization time τ_f , computed from the peak location in strain fluctuations, as a function of the applied stress (σ_0) for different system sizes: using open circles for $N=17576$ and open square for $N=1600$. The dashed lines show fit using $\sim [\sigma_0 - \sigma_c]^{-\zeta}$, obtaining $\sigma_c \approx 0.0772(N = 17576), 0.0801(N = 1600)$, with $\zeta = 2.66$. Also shown, using filled circles, is the fluidization time, τ_f^{ss} , obtained from the moment of reaching constant $\partial_t \gamma_{av}$, with the dashed line corresponding to a similar fit as above, with $\sigma_{ss} \approx 0.084$, $\zeta_{ss} = 2.18$.

shown in Fig. 7(b), using filled symbols. In this case, also, a divergence is observed (corresponding fit is shown in Fig. 7(b)), and the estimated stress threshold for onset of flow comes out to be $\sigma_{ss} \approx 0.084$, which is close to the estimated dynamical threshold $\sigma_d \approx 0.083$, obtaining also an exponent $\zeta_{ss} = 2.18$. For the smaller system, it becomes difficult to have a good quality measurement, using this definition, due to lot of fluctuations in the response.

We note, here, that all such estimates of the threshold or the exponent for divergence are subject to accuracy in measuring the timescale, by using any of the above definitions, and this measurement is strongly subject to proper averaging over a large enough ensemble of initial states, for each system size. Nevertheless, our observation that yielding threshold decreases with increasing system size is consistent with experimental measurements⁵¹, and also the hypothesis that within a larger system, there is more likelihood of finding a weak zone that would lead to earlier yielding, as compared to a smaller system. This has also been observed for crystal plasticity^{2,52}. In any case, more numerical investigations are needed to clarify this in the context of yielding of amorphous systems.

6 Concluding discussion

In this paper, we have studied several statistical aspects of the creep response of a model soft glass by means of particle based simulations. We propose a novel method to impose a target shear stress to the system, using periodic boundary conditions, which allows for studying the bulk rheology under applied shear stress, and we tested the robustness of this approach in details. This over-constrained method for applying the shear combined with our feedback mechanism allows for the study of the bulk dynamics of a system undergoing creep without imposing a particular flow profile. In this way, we are able to address questions like finite size effects in the dynamics without having to deal with

over-constraint dynamics or unwanted wall effects.

We use this method on a three dimensional binary mixture of particles interacting via a Yukawa potential to be able to compare to earlier works, that had been implemented with walls⁹. The resulting mechanical response takes the form of a usual creep curve with a fast elastic response followed by a power-law decay of the strain rate, with exponents that lie in the typical range of experiments and earlier simulations. At longer times, depending on the stress applied we see a rapid acceleration of the deformation rate, eventually leading to a steady flow. We show that the corresponding flow curve for this steady flow agree with the one from strain rate controlled protocols, thus validating the protocol.

By investigating the compliance curves, we demonstrate how to evidence the onset of plasticity that occurs above a given value of the compliance, independent of the applied stress and system size. The subsequent plastic regime exhibits finite size effects. In this regime, the dependence on the system size becomes stronger as we lower the applied stress value, approaching the yielding transition.

Next, we demonstrate that the sample-to-sample fluctuations of the strain curves show a strong non-monotonic behavior and we identify the prominent peak observed in these fluctuations as a precursor for fluidisation. Since the position of this peak as a function of strain appears neither stress nor system size dependent, we use this feature to unambiguously define a fluidisation time that we measure as a function of imposed stress and system size.

The analysis of the fluidisation time dependence on the imposed external shear stress suggests a divergence of the time to reach a flowing state close to the yield threshold. Although more statistics will be necessary to be more conclusive and obtain quantitative relations, the system size analysis of the fluidisation time seems to indicate that smaller systems exhibit a longer fluidisation times. This result is in agreement with the weakest link theory, that predicts that smaller systems exhibit a larger strength, since the smaller the sample, the smaller also the probability to encounter a weak spot, that would lead to failure^{2,52}.

The above observations, related to size effects, as well as the strongly intermittent dynamics, observed in the individual creep curves for small applied stress and small system size, are likely related to the development of dynamical heterogeneities, with increasing spatial scale, close the yield threshold. Such stick-slip behaviour is also reminiscent of avalanche type dynamics for the plasticity close to the yielding point^{29,30}. All these would indicate strongly correlated dynamics, with decreasing stress, in tune with the hypothesis that yielding corresponds to an underlying dynamical phase transition, accompanied by critical dynamics^{31,32}. Further extensive investigations are necessary to test out these ideas and the numerical protocol, described here, would be an useful mode for such studies.

7 Acknowledgements

K. M. and P. C. acknowledge financial support from CEFIPRA Grant No. 5604-1 (AMORPHOUS-MULTISCALE). K. M. and R. C. acknowledge financial support under ANR Grant No. ANR-14-CE32-0005 (FAPRES). Part of the computations pre-

sented in this paper were performed using the CIMENT infrastructure (<https://ciment.ujf-grenoble.fr>), which is supported by the Rhône-Alpes region (GRANT CPER07_13 CIRA: <http://www.ci-ra.org>) and the CURIE cluster at TGCC thanks to the Grand Equipement National de Calcul Intensif Project No. t201509747. We also acknowledge the use of HPC facilities at IMSc, Chennai, for our computations. Further we thank Jean-Louis Barrat, Eric Bertin and Luca Cipelletti for interesting discussions on the topic.

References

- 1 D. Bonn and M. M. Denn, *Science*, 2009, **324**, 1401–1402.
- 2 S. Zapperi, *The European Physical Journal B*, 2012, **85**, 329.
- 3 M. Ozawa, L. Berthier, G. Biroli, A. Rosso and G. Tarjus, *Proceedings of the National Academy of Sciences*, 2018, 201806156.
- 4 M. Popović, T. W. de Geus and M. Wyart, *arXiv preprint arXiv:1803.11504*, 2018.
- 5 P. J. Skrzyszewska, J. Sprakel, F. A. de Wolf, R. Fokkink, M. A. Cohen Stuart and J. van der Gucht, *Macromolecules*, 2010, **43**, 3542–3548.
- 6 T. Divoux, C. Barentin and S. Manneville, *Soft Matter*, 2011, **7**, 8409.
- 7 A. Pons, T. Darnige, J. Crassous, E. Clément and A. Amon, *EPL (Europhysics Letters)*, 2016, **113**, 28001.
- 8 T. Sentjabrskaja, P. Chaudhuri, M. Hermes, W. Poon, J. Horbach, S. Egelhaaf and M. Laurati, *Scientific reports*, 2015, **5**, 11884.
- 9 P. Chaudhuri and J. Horbach, *Physical Review E - Statistical, Nonlinear, and Soft Matter Physics*, 2013, **88**, 1–5.
- 10 B. J. Landrum, W. B. Russel and R. N. Zia, *Journal of Rheology*, 2016, **60**, 783–807.
- 11 J. L. Lebowitz, *Annual Review of Physical Chemistry*, 1968, **19**, 389–418.
- 12 D. Ruelle, *Statistical mechanics: Rigorous results*, World Scientific, 1999.
- 13 O. Penrose, *Markov Processes Relat. Fields*, 2002, **8**, 351–364.
- 14 F. Sausset, G. Biroli and J. Kurchan, *Journal of Statistical Physics*, 2010, **140**, 718–727.
- 15 S. Saw and P. Harrowell, *Physical review letters*, 2016, **116**, 137801.
- 16 S. Saw, S. Abraham and P. Harrowell, *Physical Review E*, 2016, **94**, 022606.
- 17 P. Nath, S. Ganguly, J. Horbach, P. Sollich, S. Karmakar and S. Sengupta, *Proceedings of the National Academy of Sciences*, 2018, **115**, E4322–E4329.
- 18 M.-C. Miguel, A. Vespignani, M. Zaiser and S. Zapperi, *Physical review letters*, 2002, **89**, 165501.
- 19 T. Bauer, J. Oberdisse and L. Ramos, *Physical review letters*, 2006, **97**, 258303.
- 20 T. Divoux, C. Barentin and S. Manneville, *Soft Matter*, 2011, **7**, 9335.
- 21 M. Leocmach, C. Perge, T. Divoux and S. Manneville, *Physical Review Letters*, 2014, **113**, 1–5.
- 22 P. Ballesta and G. Petekidis, *Physical Review E*, 2016, **93**, 042613.
- 23 C. Liu, K. Martens and J.-L. Barrat, *Physical Review Letters*, 2018, **120**, 028004.
- 24 D. Bonn, M. M. Denn, L. Berthier, T. Divoux and S. Manneville, *Reviews of Modern Physics*, 2017, **89**, 035005.
- 25 A. Nicolas, E. E. Ferrero, K. Martens and J.-L. Barrat, *arXiv preprint arXiv:1708.09194*, 2017.
- 26 A. Jaishankar and G. H. McKinley, *Proc. R. Soc. A*, 2013, p. 20120284.
- 27 S. Aime, L. Cipelletti and L. Ramos, *arXiv preprint arXiv:1802.03820*, 2018.
- 28 G. P. Shrivastav, P. Chaudhuri and J. Horbach, *Physical Review E*, 2016, **94**, 042605.
- 29 K. M. Salerno, C. E. Maloney and M. O. Robbins, *Physical Review Letters*, 2012, **109**, 105703.
- 30 M. Talamali, V. Petäjä, D. Vandembroucq and S. Roux, *Physical Review E*, 2011, **84**, 016115.
- 31 J. Lin, E. Lerner, A. Rosso and M. Wyart, *Proceedings of the National Academy of Sciences*, 2014, **111**, 14382–14387.
- 32 C. Liu, E. E. Ferrero, F. Puosi, J.-L. Barrat and K. Martens, *Physical review letters*, 2016, **116**, 065501.
- 33 V. Gopalakrishnan and C. Zukoski, *Journal of Rheology*, 2007, **51**, 623–644.
- 34 T. Gibaud, D. Frelat and S. Manneville, *Soft Matter*, 2010, **6**, 3482–3488.
- 35 S. Lindström, T. Kodger, J. Sprakel and D. Weitz, *Soft Matter*, 2012.
- 36 S. Merabia and F. Detcheverry, *EPL (Europhysics Letters)*, 2016, **116**, 46003.
- 37 J. Zausch and J. Horbach, *EPL (Europhysics Letters)*, 2009, **88**, 60001.
- 38 T. Soddemann, B. Dünweg and K. Kremer, *Physical Review E*, 2003, **68**, 046702.
- 39 R. D. Groot and P. B. Warren, *The Journal of Chemical Physics*, 1997, **107**, 4423–4435.
- 40 T. A. Vezirov, S. Gerloff and S. H. L. Klapp, *Soft Matter*, 2015, **11**, 406–413.
- 41 S. Plimpton, *Journal of computational physics*, 1995, **117**, 1–19.
- 42 F. Varnik, L. Bocquet and J.-L. Barrat, *The Journal of chemical physics*, 2004, **120**, 2788–2801.
- 43 G. P. Shrivastav, P. Chaudhuri and J. Horbach, *Journal of Rheology*, 2016, **60**, 835–847.
- 44 V. V. Vasisht, G. Roberts and E. Del Gado, *arXiv preprint arXiv:1709.08717*, 2017.
- 45 M. Siebenbürger, M. Ballauff and T. Voigtmann, *Physical review letters*, 2012, **108**, 255701.
- 46 C. Baravian and D. Quemada, *Rheologica acta*, 1998, **37**, 223–233.
- 47 R. H. Ewoldt and G. H. McKinley, *Rheol. Bull.*, 2007, **76**, 4–6.
- 48 C. Christopoulou, G. Petekidis, B. Erwin, M. Cloitre and D. Vlassopoulos, *Philosophical Transactions of the Royal Society of London A: Mathematical, Physical and Engineering Sciences*,

- 2009, **367**, 5051–5071.
- 49 K. Nijenhuis, G. McKinley, S. Spiegelberg, H. Barnes, N. Aksel, L. Heymann and J. Odell, in *Springer Handbook of Experimental Fluid Mechanics*, Springer, 2007, pp. 619–743.
- 50 J. Rosti, J. Koivisto, L. Laurson and M. J. Alava, *Physical review letters*, 2010, **105**, 100601.
- 51 J. Weiss, L. Girard, F. Gimbert, D. Amitrano and D. Vandembroucq, *Proceedings of the National Academy of Sciences*, 2014, 201403500.
- 52 P. D. Ispánovity, Á. Hegyi, I. Groma, G. Györgyi, K. Ratter and D. Weygand, *Acta Materialia*, 2013, **61**, 6234–6245.